Journal of Molecular and Cellular Cardiology 185 (2023) 26–37

Contents lists available at ScienceDirect

Journal of Molecular and Cellular Cardiology

journal homepage: www.elsevier.com/locate/yjmcc

Nonsense mediated decay factor UPF3B is associated with cMyBP-C haploinsufficiency in hypertrophic cardiomyopathy patients

Valentin Burkart [a,*], Kathrin Kowalski [a], Alina Disch [a], Denise Hilfiker-Kleiner [b,1], Sean Lal [c], Cristobal dos Remedios [d], Andreas Perrot [e], Andre Zeug [f], Evgeni Ponimaskin [f], Maike Kosanke [g], Oliver Dittrich-Breiholz [g], Theresia Kraft [a], Judith Montag [a]

[a] Institute for Molecular and Cell Physiology, Hannover Medical School, Hannover, Germany
[b] Clinic of Cardiology and Angiology, Hannover Medical School, Hannover, Germany
[c] School of Medical Sciences, Faculty of Medicine and Health, University of Sydney, Sydney, Australia
[d] Mechanosensory Biophysics Laboratory, Victor Chang Cardiac Research Institute, Darlinghurst, NSW, Australia
[e] Charité – Universitätsmedizin Berlin, Experimental & Clinical Research Center, Berlin, Germany
[f] Institute of Neurophysiology, Hannover Medical School, Hannover, Germany
[g] Research Core Unit Genomics, Hannover Medical School, Hannover, Germany

ARTICLE INFO

Keywords:
Hypertrophic cardiomyopathy
cMyBP-C haploinsufficiency
Nonsense mediated mRNA decay
UPF3B

ABSTRACT

Hypertrophic cardiomyopathy (HCM) is the most prevalent inherited cardiac disease. Up to 40% of cases are associated with heterozygous mutations in myosin binding protein C (cMyBP-C, *MYBPC3*). Most of these mutations lead to premature termination codons (PTC) and patients show reduction of functional cMyBP-C. This so-called haploinsufficiency most likely contributes to disease development.

We analyzed mechanisms underlying haploinsufficiency using cardiac tissue from HCM-patients with truncation mutations in *MYBPC3* ($MYBPC3_{trunc}$). We compared transcriptional activity, mRNA and protein expression to donor controls. To differentiate between HCM-specific and general hypertrophy-induced mechanisms we used patients with left ventricular hypertrophy due to aortic stenosis (AS) as an additional control. We show that cMyBP-C haploinsufficiency starts at the mRNA level, despite hypertrophy-induced increased transcriptional activity. Gene set enrichment analysis (GSEA) of RNA-sequencing data revealed an increased expression of NMD-components. Among them, Up-frameshift protein UPF3B, a regulator of NMD was upregulated in $MYBPC3_{trunc}$ patients and not in AS-patients. Strikingly, we show that in sarcomeres UPF3B but not UPF1 and UPF2 are localized to the *Z*-discs, the presumed location of sarcomeric protein translation. Our data suggest that cMyBP-C haploinsufficiency in HCM-patients is established by UPF3B-dependent NMD during the initial translation round at the *Z*-disc.

1. Introduction

Hypertrophic Cardiomyopathy (HCM) is the most frequent inherited cardiac disease, characterized by asymmetric hypertrophy of the left ventricle and the interventricular septum. In about half of the patients with HCM, causative mutations can be identified. These mutations occur in different sarcomeric and some rarely affected non-sarcomeric genes and almost all patients are heterozygous for the respective mutation [1,2]. The most frequently affected genes are *MYBPC3* encoding for the cardiac myosin binding protein C (cMyBP-C) and *MYH7* encoding for the β-myosin heavy chain [2]. Some mutations alter protein function thereby inducing a poison peptide effect, while other mutations result in a reduction of total functional protein, leading to haploinsufficiency of the affected protein. Interestingly, the majority of HCM-causing *MYBPC3*-mutations lead to premature termination codons (PTC) either through nonsense, frameshift or splice variants [3–5]. However, truncated cMyBP-C fragments expressed from the mutated allele have not been detected in patients with *MYBPC3* truncation ($MYBPC3_{trunc}$) mutations [6–10]. This lack of truncated cMyBP-C was in most cases accompanied by an overall reduction of total cMyBP-C [6–8,11]. Two

* Corresponding author at: Carl-Neuberg-Straße 1, 30625 Hannover, Germany.
E-mail address: burkart.valentin@mh-hannover.de (V. Burkart).
[1] Current address: Institute of Cardiovascular Complications in Pregnancy and in Oncologic Therapies, Philipps-University Marburg, Germany

https://doi.org/10.1016/j.yjmcc.2023.09.008
Received 15 May 2023; Received in revised form 8 September 2023; Accepted 28 September 2023
Available online 4 October 2023

different cellular mechanisms could explain this reduction, which could work separately from each other or in combination. First, the newly produced truncated cMyBP-C could be degraded via the ubiquitin proteasome system [12,13]. Second, the translational stop at the PTC could induce nonsense mediated mRNA decay (NMD) of the mutated *MYBPC3*-mRNA (reviewed in [14,15]). It was previously discussed, that both degradation pathways could work in parallel [16].

Some studies have previously shown reduced amounts of *MYBPC3*-mRNA, therefore involvement of NMD seems more plausible [6–8]. NMD is a complex quality control pathway for mRNA transcripts containing PTCs. Upon premature translation termination, activation of NMD is triggered by different mechanisms [17,18]. Among them, Up-frameshift protein (UPF)-dependent NMD plays an important role. In eukaryotes, three UPF proteins are expressed, UPF1, 2, and 3, and humans express two paralogues of UPF3, UPF3A, and UPF3B. UPF1 has been shown to be essential in RNA quality control, where it has several roles. It binds to chromatin in the nucleus and promotes transcription-coupled NMD [19] and in addition, it can directly bind to RNA where it has been shown to concentrate in 3'UTR if a PTC and a 3'UTR exon junction complex (EJC) is present [20,21]. UPF1 triggers NMD after it is phosphorylated and interacts with SMG5, 6 and 7 [20,22,23]. Another branch of NMD-activation involves the EJC, which is placed upon mRNA splicing 20–24 nucleotides upstream of each splice site [24]. Physiologically, EJC's are removed during the initial round of translation thereby stabilizing the mRNA for further translation. If a PTC is located >50–55 nucleotides upstream of an exon-exon junction, the downstream EJCs are not removed during the initial translation [25,26]. Current models imply that spliced mRNAs with associated exon-junction complexes are shuttled to the cytoplasm where UPF1 binds to the mRNA and UPF3B binds to proteins of the EJC. During the initial round of translation, the UPF1-UPF3B complex initiates translation termination if the ribosome encounters a PTC [27]. Depending on the EJC-composition, this can either lead to direct activation of NMD (UPF2-independent NMD) or to recruitment of UPF2 and subsequent activation of NMD by UPF2 [28]. EJCs are bridged to RNA-bound UPF1 by UPF2 or UPF3B leading to UPF1 phosphorylation through SMG1 kinase thereby initiating NMD ([29] and reviewed in [14]).

Apart from its role as transcript quality control mechanism, NMD can regulate gene expression, maturation, and differentiation during embryonic development and influence cell stress responses (reviewed in [30,31]). For example, alternative splicing of gene transcripts can lead to mRNAs targeted by NMD and thereby regulate mRNA abundance of these genes (reviewed in [32]). Furthermore, inhibition of NMD can stabilize the transcripts of several stress-induced genes and thereby augment the cellular stress response [33].

To date, it is still not fully understood how HCM disease development is triggered in patients with *MYBPC3*$_{trunc}$ mutations, since cMyBP-C protein levels are not always reduced [34,35]. Recently, it was hypothesized, that chronic activation of NMD might contribute to HCM disease development [36,37]. Since NMD is connected to various cellular pathways like cell differentiation, autophagy as well as gene expression regulation [31], it is conceivable, that alterations of NMD-activity could affect cardiomyocyte (CM) functionality and thereby induce HCM.

Involvement of NMD in mutant *MYBPC3*-mRNA degradation was found in cMyBP-C knock-in mice [16]. Furthermore, upregulation of NMD-pathway was determined in *MYBPC3*$_{trunc}$ iPSC-CMs [37]. The marked total *MYBPC3*-mRNA or mutant *MYBPC3*-mRNA reduction, which occurs in *MYBPC3*$_{trunc}$ patients with HCM [6–8,34] suggests that degradation of mutated *MYBPC3*-mRNA via NMD is responsible for the reduction . However, a direct link between cMyBP-C haploinsufficiency and NMD has not yet been shown in HCM-patients with *MYBPC3*$_{trunc}$ mutations.

The aim of this study was therefore, to investigate whether NMD is associated with *MYBPC3* gene and protein expression in HCM-patients with different *MYBPC3*$_{trunc}$ mutations in comparison to heart-healthy donors and to patients with left ventricular hypertrophy due to aortic stenosis (AS). We show that changes of the cMyBP-C protein level are directly correlated with *MYBPC3* transcript level, whereas increased transcriptional activity is associated with hypertrophic growth of the heart. Therefore, we conclude that degradation of mutant mRNA via NMD represents the underlying mechanism of cMyBP-C haploinsufficiency. We provide additional evidence that UPF3B plays a central role in *MYBPC3*-NMD and that it could take place at the *Z*-discs in CMs.

2. Material and methods

2.1. Patients and donors

The study on anonymized human tissue was approved by the ethics committee of Hannover Medical School and experiments were carried out in accordance with the given recommendations (No. 2276–2014). Written informed consent according to the Declaration of Helsinki [38] was given by all subjects.

Left ventricular septum tissue from HCM-patients was obtained either during myectomy surgery or after heart transplantation. We analyzed patients diagnosed with hypertrophic obstructive cardiomyopathy (HOCM) as evident from increased septal thickness (>13 mm) in the absence of overt causes for hypertrophy. Furthermore, we analyzed patients with left ventricular hypertrophy due to aortic stenosis of whom cardiac tissue was also obtained by myectomy (Morrow procedure). Non-transplanted hearts from donors without any known cardiovascular condition were obtained from the Sydney Heart Bank [39]. Detailed information on mutations and clinical characteristics are given in Supplement Table 1.

2.2. Analysis of HCM-patient samples for truncated cMyBP-C fragments and protein content

Relative cMyBP-C protein amounts were quantified as described previously [40]. Briefly, cardiac tissue samples from donors and patients were ground in a cryo-mortar and re-suspended in sample buffer. Protein separation was performed by polyacrylamide gel electrophoresis and subsequent transfer to a nitrocellulose membrane (GE10600001; GE Healthcare) for cMyBP-C and UPF3B quantification and to a PVDF membrane (88518; ThermoFisher Scientific) for UPF1 and UPF2 quantification by western blotting. The following antibodies were used for detection of cMyBP-C (N-terminus; sc137237; Santa Cruz; dilution 1:500), α-actinin (ab9465; Abcam; 1:1000), cTnI (29863; Biogenes; 1:500), UPF1 (NBP1–89641; Novusbio; dilution 1:100), UPF2 (NBP2–57706; Novusbio; dilution 1:100), and UPF3B (NBP1–83134; Novusbio; dilution 1:100).

2.3. Relative MYBPC3-mRNA quantification via RT-qPCR

Total RNA was extracted using the 'Monarch® Total RNA Miniprep Kit' (T2010S; NEB) from frozen cardiac tissue of donors and patients ground in a cryo-mortar. RNA was reverse transcribed in 14.5 µl total reaction volume containing either 2.5 µM random decamers (AM5722G; ThermoFisher Scientific) for *MYBPC3*-mRNA quantification and 0.5 µM specific reverse transcription primers for *UPF3B*-mRNA quantification (listed in Supplement Table 2), 5 U Tetro reverse transcriptase (BIO-65050; Bioline), 1 U RNase inhibitor (BIO-65028; Bioline) and 500 µM dNTPs (R0192; Fermentas) incubated for 1 h at 42 °C. Expression of *MYBPC3* and *TNNI3* was analyzed in a multiplex quantitative PCR assay for relative *MYBPC3*-mRNA quantification. For *UPF3B*-mRNA quantification, expression of *UPF3B* was analyzed in a multiplex quantitative PCR assay together with *GAPDH*. 1× TaqMan™ Universal Mastermix II, no UNG (4440040; ThermoFisher Scientific) was used together with 0.25 µM primers and 0.0625 µM probes all ordered from Biomers and listed in Supplement Table 2, in a final volume of 20 µl in duplicates. The

standard protocol from the QuantStudio™ 6 Flex System (ThermoFisher Scientific) was used with initial 95 °C for 10 min followed by 40 cycles of 95 °C for 15 s and 60 °C for 45 s. Relative mRNA expression as fold change was calculated using the ΔΔCt-method. As reference genes, *TNNI3* was used for *MYBPC3* and *GAPDH* for *UPF3B*. Individual values were normalized to the average of the analyzed donor samples. Analyses were performed in five individual quantifications.

2.4. RNA fluorescence in situ hybridization (RNA-FISH) for detection of MYBPC3 and TNNI3 active transcription sites (aTS)

Detection of active transcription sites in CM nuclei was performed as previously described [40]. Cryosections (10–16 μm thickness) were prepared from frozen left ventricular heart tissue and hybridized with fluorescently labeled sets of 20-mer oligonucleotides (LGC Biosearch Technologies) for intronic or exonic sequences of *MYBPC3*- and *TNNI3*-RNA, respectively. Probe sets for intronic pre-mRNA labeled with fluorophore Quasar 670 (LGC Biosearch Technologies) and exonic mRNA probe sets with fluorophore Quasar 570 (LGC Biosearch Technologies) were custom designed (Stellaris® Probe Designer, as published in [40]). Co-localization of both Quasar 570 and Quasar 670 fluorescence in CM nuclei indicate active transcription sites (aTS). For each analyzed individual, aTS in at least 80 nuclei were counted. aTS/nucleus were calculated as measure for transcriptional activity. *MYBPC3* aTS/nucleus for patients H36, H45, and H84 were derived from previously published data in [40].

2.5. RNA-sequencing

Extracted RNA described under 'relative *MYBPC3*-mRNA quantification' was used for cDNA-library generation and subsequent RNA-sequencing. Primary quality control of the RNA samples showed substantial levels of small fragments <200 nucleotides. In order not to risk any negative impact on library generation, an additional purification step using magnetic beads was implemented to effectively remove these short fragments. cDNA-library generation, RNA-sequencing, and raw data processing was performed by the Research Core Unit Genomics (RCUG) of Hannover Medical School. 40 ng of total RNA per sample (differing for sample H66 (31 ng), H88 (37 ng), H36 (35 ng), H154 (37 ng), and H125 (32 ng) due to limited sample material for RNA extraction) were utilized as input for mRNA enrichment procedure with 'NEBNext® Poly(A) mRNA Magnetic Isolation Module' (E7490L; New England Biolabs) followed by stranded cDNA library generation using 'NEBNext® Ultra II Directional RNA Library Prep Kit for Illumina' (E7760L; New England Biolabs). All steps were performed as recommended in user manual E7760 (Version 1.0_02–2017; NEB) with downscaling of all reactions to 2/3 of initial volumes. Furthermore, one additional purification step was introduced at the end of the standard procedure, using 1.2× 'Agencourt® AMPure® XP Beads' (A63881; Beckman Coulter, Inc.). cDNA libraries were barcoded by dual indexing approach, using 'NEBNext Multiplex Oligos for Illumina – 96 Unique Dual Index Primer Pairs' (6440S; New England Biolabs). All generated cDNA libraries were amplified with 12 cycles of final PCR. Fragment length distribution of individual libraries was monitored using 'Bioanalyzer High Sensitivity DNA Assay' (5067–4626; Agilent Technologies). Quantification of libraries was performed by use of the 'Qubit® dsDNA HS Assay Kit' (Q32854; ThermoFisher Scientific). Equal molar amounts of 21 individually barcoded libraries were pooled for a collective sequencing run. The library pools were denatured with NaOH and were finally diluted to 2 pM. 1.3 ml of each denatured pool was loaded on an Illumina NextSeq 550 sequencer using a High Output Flowcell for single reads (20024906; Illumina). Sequencing was performed with the following settings: Sequence reads 1 and 2 with 38 bases each; Index reads 1 and 2 with 8 bases each. BCL files were converted to FASTQ files using bcl2fastq Conversion Software version v2.20.0.422 (Illumina). Raw data processing was conducted by use of nfcore/rnaseq (version 1.4.2). The pipeline uses Nextflow, as bioinformatics workflow tool to pre-process raw data from FastQ inputs, align reads, and perform extensive quality-control on the results. The genome reference and annotation data were taken from GENCODE.org (*Homo sapiens*; GRCh38.p13; release 34). Normalization and differential expression analysis were performed on the internal Galaxy (version 20.05) instance of the RCU Genomics, Hannover Medical School, Germany with DESeq2 (Galaxy Tool Version 2.11.40.6) with default settings except for "Output normalized counts table", which was set to "Yes" and all additional filters were disabled ("Turn off outliers replacement", "Turn off outliers filtering", and "Turn off independent filtering" set "Yes").

2.6. Allelic quantification of MYBPC3-mRNA with RNA-sequencing results

We quantified the relative amount of mutant *MYBPC3*-mRNA in the $MYBPC3_{trunc}$ patients in our RNA-sequencing data. For patients H36, H44, and H51 with exonic mutations ($MYBPC3_{c.2864\_2865delCT}$, $MYBPC3_{c.3697C>T}$, and $MYBPC3_{c.1700\_1701delAG}$,) we could directly compare the read counts of mutant to wildtype transcripts and calculate the percentage of each. For patients H45, H59, and H84 ($MYBPC3_{c.1458-6G>A}$, $MYBPC3_{c.3490+1G>T}$, and $MYBPC3_{c.927-2A>G}$) where mutations are located in introns, we calculated the percentage of mutated reads relative to the mean reads of two random positions in the upstream and two in the downstream exons of the affected intron.

2.7. IsoformSwitchAnalyzeR

Sequencing raw data was processed using nfcore/rnaseq (version 3.6) with default parameters to retrieve spliced aware genome alignment and count quantification on transcript level. Salmon transcript level quantification of the samples was introduced to IsoformSwitchAnalyzeR (version 1.20.0) and analyzed using IsoformSwitchAnalysisCombined function with default parameters according to the vignette (https://bioconductor.org/packages/devel/bioc/vignettes/IsoformSwitchAnalyzeR/inst/doc/IsoformSwitchAnalyzeR.html#how-to-prevent-visualization-of-nmd-in-the-switchplot) for identification of isoform switches.

2.8. Gene set enrichment analysis (GSEA)

The gene set enrichment analysis (GSEA) was performed using the software package from UC San Diego and Broad Institute (version 4.1.0). We used the output of the DESeq2 analysis from RNA-sequencing and compared that to the reactome gene set database version 7.4 (c2.cp.reactome.v7.4.symbols.gmt [curated]). Analysis was performed with 1000 permutations and the permutation type was set to "gene_set".

2.9. Immunofluorescence staining of cardiac tissue cryosections

Immunofluorescence staining of cardiac tissue cryosections was performed as previously described [40]. In short, cryosections (5 μm thick) from donor and $MYBPC3_{trunc}$ patient cardiac tissue were fixed in 4% paraformaldehyde and antibodies against UPF1 (NBP1–89641; Novusbio; dilution 1:100), UPF2 (NBP2–57706; Novusbio; dilution 1:100), and UPF3B (NBP1–83134; Novusbio; dilution 1:100) in combination with α-actinin (A7811; Sigma; dilution 1:100) were incubated for 1 h at room temperature. As secondary antibodies, anti-mouse Alexa Fluor 488 (A2102; ThermoFisher Scientific; dilution 1:400) and anti-rabbit Alexa Fluor 555 (A31572; ThermoFisher Scientific; 1:400) were applied simultaneously. DAPI was used to stain nuclei. Cryosections were analyzed by confocal laser scanning microscopy (Zeiss LSM).

2.10. Statistical analysis

Values are presented as mean ± SD unless indicated otherwise. In multi-group comparisons one-way analysis of variance (ANOVA) and Tukey's *post-hoc* test was applied. Significance for all tests was accepted when $p < 0.05$. Statistical analysis and linear correlation test (Pearson correlation coefficient) was performed using GraphPad Prism (version 9.5.0).

3. Results

3.1. cMyBP-C haploinsufficiency disrupts sarcomeric stoichiometry in *MYBPC3*$_{trunc}$ patients

We compared cMyBP-C protein expression in tissue samples from HCM-patients with truncation mutations in cMyBP-C, donors, and patients with aortic stenosis (AS). To ensure that only patients with haploinsufficiency were included in our study, we used western blot analysis to quantify cMyBP-C protein levels. We performed six individual western blot analyses for four *MYBPC3*$_{trunc}$ patients with mutations *MYBPC3*$_{c.3288delG}$ (H34), *MYBPC3*$_{c.3697C>T}$ (H44), *MYBPC3*$_{c.1700\_1701delAG}$ (H51), and *MYBPC3*$_{c.3490+1G>T}$ (H59) and included patients H36 (*MYBPC3*$_{c.2864\_2865delCT}$), H45 (*MYBPC3*$_{c.1458-6G>A}$), and H84 (*MYBPC3*$_{c.927-2A>G}$) analyzed in [40], five donors (H88, H89, H103, H108, H113) and four patients with AS (H69, H125, H126 and H130). Overall, *MYBPC3*$_{trunc}$ patients showed reduced cMyBP-C amounts compared to donors and AS-patients, whereas both, α-actinin and cTnI where expressed at comparable levels among the individuals (Fig. 1A). Quantitative analysis confirmed this finding. When normalized to the expression of α-actinin, a protein of the *Z*-disc, *MYBPC3*$_{trunc}$ patients showed on average a significant reduction by 27% compared to donors and by 23% compared to AS-patients, indicating haploinsufficiency in the HCM-patients. Proteins of the thin and thick filament are expressed in a fixed stoichiometry for proper function (reviewed in [42]). Therefore, haploinsufficiency could affect this stoichiometry and thereby sarcomeric function. To examine whether stoichiometry was affected, we normalized cMyBP-C expression also to cTnI. We detected a comparable and significant reduction in cMyBP-C by 27% and 36% in comparison to donors and AS-patients. In contrast, AS-patients showed no significant deviation from donor samples in cMyBP-C expression (Fig. 1B). This indicates that sarcomeric stoichiometry is affected in *MYBPC3*$_{trunc}$ but not in AS-patients. To analyze overall reduction in cMyBP-C in cardiac tissue, we compared cMyBP-C expression relative to β-tubulin, a non-sarcomeric protein which is expressed in cardiomyocytes and non-myocytes (Supplement Fig. 1). Here, we detected an even higher reduction in cMyBP-C of 58% on average. This could

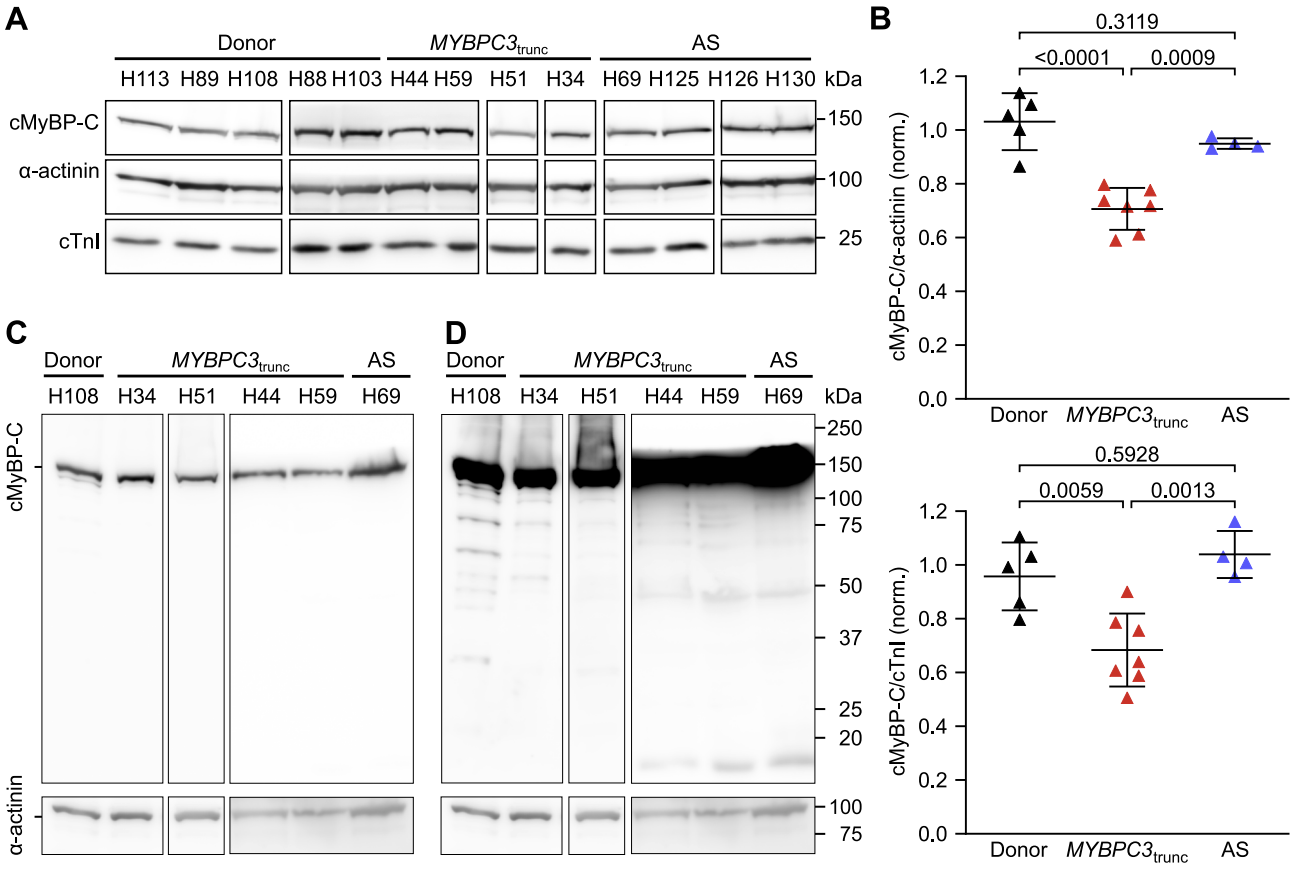

Fig. 1. cMyBP-C haploinsufficiency in *MYBPC3*$_{trunc}$ patients.
Protein extracts from frozen tissue samples were analyzed on western blots after SDS-PAGE. **A** Exemplary western blot for quantification of cMyBP-C relative to α-actinin or cTnI. Each membrane was cut into three pieces and incubated with the respective antibody. **B** Relative quantification of cMyBP-C to α-actinin or cTnI from six individual western blot membranes. Each triangle represents the mean of the six experiments for each individual. Analyzed individuals were H88, H89, H103, H108, and H113 in the donor group, H34, H44, H51, and H59 together with previously published results from H36, H45, and H84 [40] in the *MYBPC3*$_{trunc}$ patient group and H69, H125, H126 and H130 in the AS-patient group. For comparison of HCM-patient results with donors or AS-patients, one-way analysis of variance (ANOVA) and Tukey's *post-hoc* test were performed. ANOVA yielded significant variation among groups ($F(2, 9) = 9.02$, $p = 0.0071$). Mean ± SD and *p*-values from Tukey's test are indicated in the fig. **C** and **D** Donor (H108), *MYBPC3*$_{trunc}$ patients (H34, H44, H51, and H59) and a patient with AS (H69) were analyzed for truncated fragments of cMyBP-C using an N-terminal cMyBP-C antibody, α-actinin was used as loading control on the same membrane. Exposure time was 5 s in **C** and 120 s in **D**.

reflect an increased β-tubulin expression in non-myocytes, e.g. due remodeling in addition to the reduction of cMyBP-C in cardiomyocytes [57]. This assumption could also explain the large scatter in cMyBP-C/β-tubulin expression in AS-patients.

In addition, western blot analysis showed no evidence for cMyBP-C fragments in the *MYBPC3*$_{trunc}$ patients (Fig. 1C). After long (120 s) exposure additional bands appeared, however these were also present in control samples from donor or AS-patients (Fig. 1D). This is in line with previous findings for patients H36, H45, and H84 where we also did not detect truncated fragments [40]. Therefore, we confirmed haploinsufficiency in our cohort of *MYBPC3*$_{trunc}$ patients and in addition showed that relative cMyBP-C levels are donor-like in the AS-patients.

3.2. Increased transcriptional activity does not compensate for reduction of MYBPC3-mRNA expression

Reduction of cMyBP-C could either be caused by reduced transcriptional activity of *MYBPC3* or by increased degradation of *MYBPC3*-mRNA and/or cMyBP-C protein. To test if the transcriptional activity of *MYBPC3* was altered in *MYBPC3*$_{trunc}$ patients, we used RNA-FISH. Probe sets against intronic and exonic RNA of *MYBPC3* and *TNNI3* were hybridized to cryosections of donors, *MYBPC3*$_{trunc}$, and AS-patients. Active transcription sites (aTS) were identified by co-localization of signals for intronic and exonic RNA in CM nuclei (Supplement Fig. 2). The number of aTS was counted per CM-nucleus and the average value of *MYBPC3* or *TNNI3* aTS/nucleus was calculated per analyzed individual. In *MYBPC3*$_{trunc}$ patients, aTS/nucleus were significantly increased for *MYBPC3* (Fig. 2A) and for *TNNI3* (Fig. 2B) as compared to donors. However, also in AS-patients transcriptional activity of both genes was increased, even though the difference was not significant. In summary, increased *MYBPC3* transcriptional activity could not explain reduced cMyBP-C levels in the *MYBPC3*$_{trunc}$ patients. Therefore, we examined if the reduction of cMyBP-C was caused by increased degradation of *MYBPC3*-mRNA. We analyzed mRNA levels of *MYBPC3* relative to *TNNI3* to detect potential changes of sarcomeric RNA stoichiometry. We extracted mRNA from cardiac tissue of all patients and donors and performed a multiplexed RT-qPCR with specific probes against *MYBPC3* and *TNNI3*. Ratios of *MYBPC3* to *TNNI3* were calculated and normalized to mean ratios of all donors. On average *MYBPC3*$_{trunc}$ patients showed a significant reduction of *MYBPC3*-mRNA relative to *TNNI3*. In AS-patients, the mean *MYBPC3/TNNI3*-mRNA ratio was not significantly reduced compared to the donor samples (Fig. 2C).

The number of *MYBPC3*-aTS/nucleus correlated negatively with *MYBPC3/TNNI3*-mRNA ratio over all analyzed individuals and showed

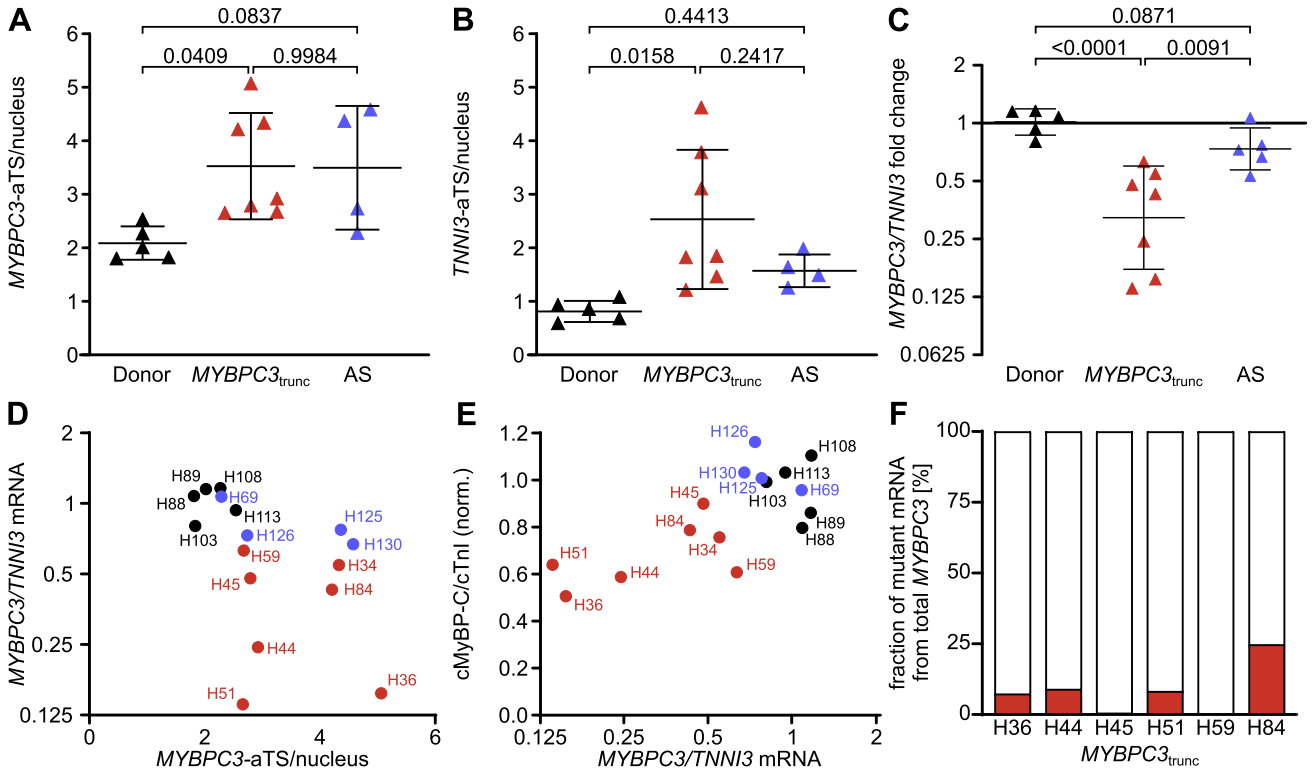

Fig. 2. Relative *MYBPC3*-mRNA expression and transcriptional activity.
Transcriptional activity of *MYBPC3* **A** and *TNNI3* **B** was quantified using RNA-FISH in cryosections from donors, *MYBPC3*$_{trunc}$ and AS-patients. The mean number of aTS/nucleus was calculated and plotted for each individual. *MYBPC3* aTS/nucleus for patients H36, H45 and H84 in **A** were derived from previously published data in [40]. ANOVA and Tukey's *post-hoc* test were performed. ANOVA yielded significant variation among groups **A** [$F(2, 13) = 5.436$, $p = 0.0192$] and **B** [$F(2, 13) = 4.394$, $p = 0.0349$]. Mean ± SD and *p*-values from Dunnett's test are indicated in the fig. **C** *MYBPC3*-mRNA was quantified in extracted RNA from donors, *MYBPC3*$_{trunc}$ and AS-patients relative to *TNNI3*. The fold change was calculated using the ΔΔCt-method with the mean of the donors as normalization. ANOVA and Tukey's *post-hoc* test were performed. ANOVA yielded significant variation among groups [$F(2, 14) = 18.65$, $p = 0.0001$]. Mean ± SD and *p*-values from Dunnett's test are indicated in the fig. **D** Correlation of *MYBPC3*-aTS/nucleus to *MYBPC3/TNNI3*-mRNA ratios as fold change per analyzed individual. Linear correlation was tested using Pearson correlation coefficient ($r = -0.5552$, $n = 16$, $p = 0.0256$). **E** Correlation of *MYBPC3/TNNI3*-mRNA ratios to cMyBP-C/α-actinin protein ratios per analyzed individual. Linear correlation was tested using Pearson correlation coefficient ($r = 0.6694$, $n = 16$, $p = 0.0046$). **F** Fraction of mutant mRNA reads as analyzed by RNA-sequencing for *MYBPC3*$_{trunc}$ patients. Mutations of patients H36, H45, and H84 cause splice site alterations. Here, fractions were calculated as reads of alternatively spliced mRNAs with the mutation per mean read counts of neighboring exons. For mutations H44, H51, and H59, which encode for a stop codon or deletions, read counts of mutant mRNA and read counts of wildtype mRNA were used for calculation of the respective fractions. Depicted are the fractions of mutant from total *MYBPC3*-mRNA as red bar from total *MYBPC3*-mRNA (100%, indicated by white stacked bars). (For interpretation of the references to colour in this figure legend, the reader is referred to the web version of this article.)

a trend to negative correlation among *MYBPC3*$_{trunc}$ patients (Fig. 2D), potentially indicating a feedback mechanism to compensate for low *MYBPC3*-mRNA levels. However, this finding underlines that changes in transcriptional activity cannot underlie haploinsufficiency. On the contrary, *MYBPC3*-mRNA levels correlated positively and significantly with the amount of cMyBP-C protein in all individuals (Fig. 2E). Therefore, reduced levels of cMyBP-C presumably occur due to a lower amount of *MYBPC3*-mRNA.

3.3. NMD-pathway is enriched in *MYBPC3*$_{trunc}$ patients

The observed reduction of *MYBPC3*-mRNA in the *MYBPC3*$_{trunc}$ patients could be explained by degradation of mutated *MYBPC3*-mRNA containing PTCs by NMD. An increased demand on NMD might result in

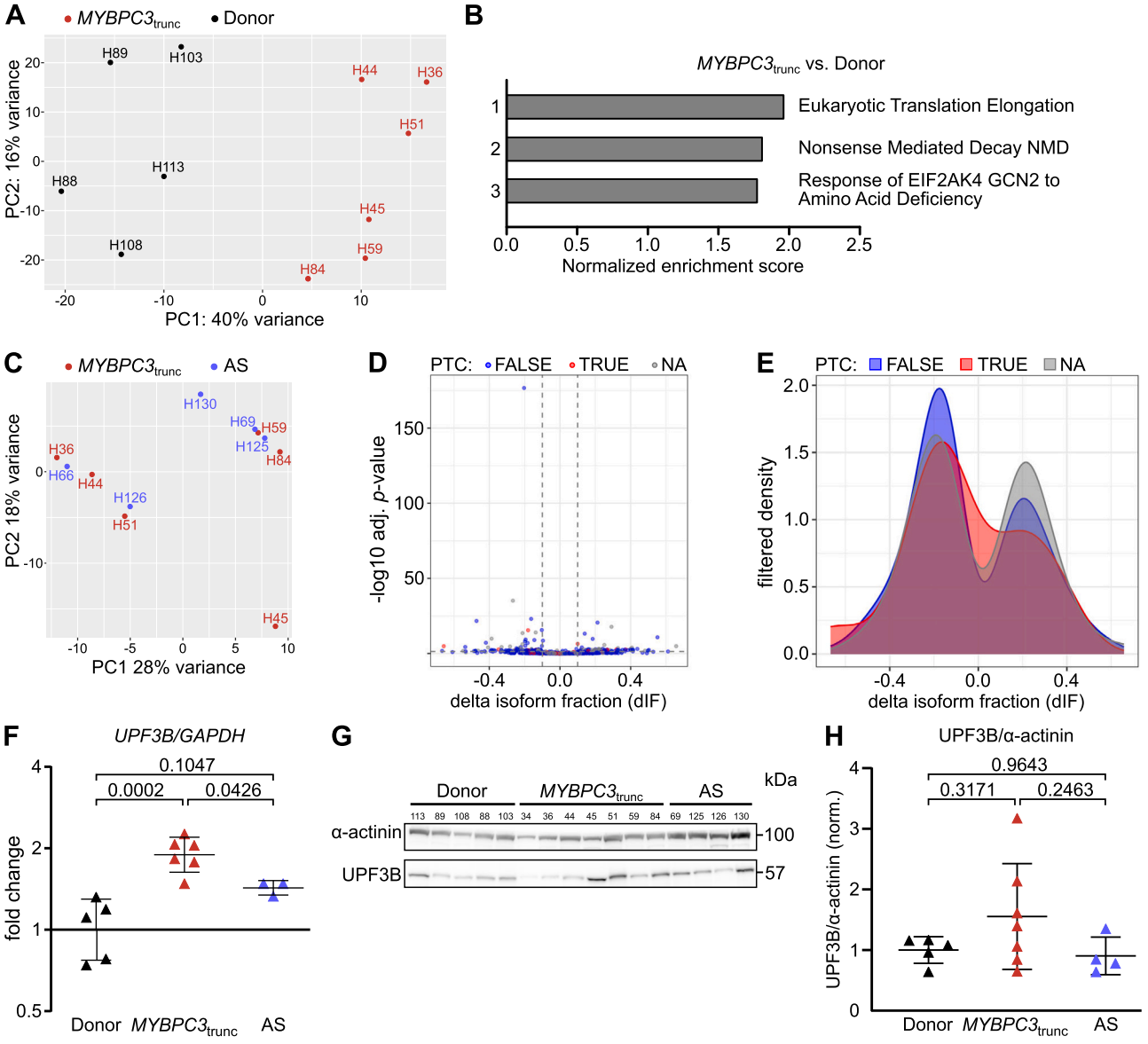

Fig. 3. Upregulation of NMD-pathway and UPF3B.
RNA isolated from donors, *MYBPC3*$_{trunc}$ and AS-patients was used for RNA-sequencing. Primary analysis was carried out using the Galaxy implemented tool DESeq2. PCA was performed and is shown here for comparison of *MYBPC3*$_{trunc}$ patients to donors **A** and to AS-patients **C**. **B** GSEA of the RNA-sequencing data presented five significantly increased gene sets with an FDR <10%. **D** Volcano plot showing the differential transcript usage (via IsoformSwitchAnalyzeR) in the RNA-sequencing data from *MYBPC3*$_{trunc}$ patients vs. donors. Isoforms containing GENCODE (release 33) annotated PTC (red TRUE), regular termination codons (blue, FALSE), or having no annotated open reading frame (gray, NA) are indicated. The change in isoform fraction (dIF) is plotted against the -log10 adjusted *p*-value **E** Density plot showing the distribution of filtered isoforms against the dIF calculated by IsoformSwitchAnalyzeR. **F** *UPF3B*-mRNA was quantified by RT-qPCR in extracted RNA from donors, *MYBPC3*$_{trunc}$ and AS-patients relative to *GAPDH*. Fold change was calculated using the ΔΔCt-method with the mean of donors as normalization. ANOVA yielded significant variation among groups showing a significant increase of *UPF3B/GAPDH* in the *MYBPC3*$_{trunc}$ patient group compared to both, donors and AS-patients ($F(2, 11) = 18.05$, $p = 0.0003$). **G** Representative western blot showing expression of UPF3B and α-actinin as loading control. Donors (H88, H89, H103; H108, H113) were compared to *MYBPC3*$_{trunc}$ (H34, H36, H44, H45, H51, H59, H84) and AS-patients (H69, H125, H126, H130). Both proteins were analyzed on the same membrane, which was cut for incubation with the respective antibody. **H** UPF3B protein was quantified relative to α-actinin via western blot. At least four independent western blots were analyzed and the mean for each individual is plotted as a triangle. ANOVA did not yield significance for the increase of UPF3B/α-actinin in the *MYBPC3*$_{trunc}$ patient group compared to donors and AS-patients most likely due to high inter-individual variability ($F(2, 13) = 1.857$, $p = 0.1953$). Mean ± SD and *p*-values from Tukey's *post-hoc* test are indicated in the figure. (For interpretation of the references to colour in this figure legend, the reader is referred to the web version of this article.)

an increased expression of NMD-components. To identify possible expression changes of NMD-pathway genes, we performed RNA-sequencing on patients with *MYBPC3*$_{trunc}$ mutations, AS-patients, and donors. The sequencing data were analyzed using the DESeq2 as Galaxy implemented tool as described in the methods section and resulted in 2208 significantly differentially expressed genes. Among them, the mean *MYBPC3*-mRNA feature counts of *MYBPC3*$_{trunc}$ patients were significantly reduced ($p = 0.0385$; mean ± SD: 50,880 ± 19,696) in comparison to donor and AS-patients groups combined (mean ± SD: 82,563 ± 15,016). Thereby, we could confirm reduction of *MYBPC3*-mRNA in the *MYBPC3*$_{trunc}$ patients. Analysis of read counts for each allele as detected by RNA-sequencing revealed only low read counts of mutant transcripts in HCM-patients (H36: 21 reads; H44: 92 reads; H45: 5 reads; H51: 50 reads; H84: 111 reads) or even none at all (H59). We used these data to calculate fractions of mutant per total *MYBPC3*-mRNA which were derived from read counts of surrounding exons. We detected allelic imbalance for each patient with substantially reduced mutant transcripts below 10% for most patients, only patient H84 showed a slightly higher mutant transcript fraction of 25%. Fractions of mutant and wildtype mRNA for each patient are presented in Fig. 2F.

Principal component analysis (PCA) of *MYBPC3*$_{trunc}$ patients vs. donors revealed a clear separation of donors from *MYBPC3*$_{trunc}$ patients into two distinct groups along PC1 with 40% of the overall variance in the data set (Fig. 3A). To reveal potentially altered gene expression pathways in *MYBPC3*$_{trunc}$ patients, a GSEA was performed using the reactome gene set database. Three gene sets were significantly enriched with a false discovery rate (FDR) <10%, containing pathways involved in metabolism of proteins (Eukaryotic Translation Elongation), metabolism of RNA (Nonsense Mediated Decay NMD), and cellular responses to stimuli (Response of EIF2AK4 GCN2 to Amino Acid Deficiency (Fig. 3B).

Interestingly, the highest variance in the data set when comparing between AS-patients and donors did not separate these two groups along PC1 and PC2, however the samples separated in two mixed groups from both, AS-patients and donors (Fig. 3C). This separation is most probably due to the sex of the analyzed individuals since all individuals from the left group are female and the right group only consists of male individuals (Supplement Table 1). Only one female *MYBPC3*$_{trunc}$ patient (H45) did not group with any of the other samples, for unknown reasons. Interestingly, this patient grouped with the other patients in the PCA *MYBPC3*$_{trunc}$ vs. donors, underlining the disease dominated separation in this comparison. Comparison of the *MYBPC3*$_{trunc}$ patients vs. the AS-patients by GSEA did only yield 45 significant differentially expressed genes and thereby no significantly enriched gene sets in GSEA.

It has been hypothesized that an increased overall demand on NMD in *MYBPC3*$_{trunc}$ patients may act as an underlying mechanism for HCM-development [16,37]. This would lead to increased amounts of PTC-containing transcripts, which would indicate disturbed or exhausted NMD. We used the R package IsoformSwitchAnalyzeR [43] to investigate the isoform fraction in the *MYBPC3*$_{trunc}$ patients compared to donors. Exhausted NMD would be indicated by a change in isoform fraction (dIF) with PTC-containing transcripts (PTC TRUE, red dots) being upregulated (top right quadrant of the volcano plot, Fig. 3D) and the respective transcripts with regular termination codons (PTC FALSE, blue) being downregulated (top left quadrant of the volcano plot, Fig. 3D). The extent of up- or downregulated transcripts with or without PTC is further visualized by the density plot (Fig. 3E), which would be expected to show a higher peak for PTC-containing transcripts with positive dIF values than for transcripts with regular termination codons. An increase of PTC-containing transcripts would indicate a disturbed NMD. However, we did not find an increase of such transcripts in the *MYBPC3*$_{trunc}$ patients in comparison to the donors (Fig. 3D and E).

3.4. NMD-component UPF3B is upregulated in *MYBPC3*$_{trunc}$ patients

GSEA of *MYBPC3*$_{trunc}$ patients vs. donors showed enrichment of the NMD gene set but also enrichment of other pathways involved in protein metabolism in the *MYBPC3*$_{trunc}$ patients compared to donors. Actually, the NMD gene set contains a total of 116 genes of which 88 overlap with the gene set of overlapping genes being ribosomal proteins. We therefore calculated the strength of regulation in *MYBPC3*$_{trunc}$ and in AS-patients of those genes that are specfic for the NMD gene set. We used the "rank metric score" calculated by the GSEA, which incorporates the strength of regulation between two analyzed groups (Supplement Table 3). When we compared our analysis of *MYBPC3*$_{trunc}$ patients vs. donors to the analysis of AS-patients vs. donors, we calculated a factor of 1.7 fold increase for the NMD-specific genes. This indicates enhanced expression of specific NMD-regulators, which could be due to the need for permanent degradation of mutated *MYBPC3*-mRNA which is absent in AS-patients.

Among the regulated NMD-specific genes, we identified *UPF3B* to be significantly ($p = 0.0010$) upregulated in *MYBPC3*$_{trunc}$ patients. To confirm upregulation of *UPF3B*, a multiplexed RT-qPCR assay was used to analyze the *UPF3B*-expression relative to *GAPDH*. The fold change of the *UPF3B/GAPDH* ratio showed a significant increase in *MYBPC3*$_{trunc}$ patients. In comparison, AS-patients showed an only modest and not significant change in *UPF3B*-expression (Fig. 3F). When analyzing UPF3B abundance at protein level we found an increased UPF3B/α-actinin ratio in the *MYBPC3*$_{trunc}$ patients but not in AS-patients compared to donors (Fig. 3G and H). The increase in UPF3B protein was less pronounced as compared to mRNA level. This is presumably due to the normalization the sarcomeric protein α-actinin, which is also expressed at higher levels due to hypertrophy. In addition, we experienced a high inter-individual variability in the *MYBPC3*$_{trunc}$ patient group, thus the increase was not statistically significant. RNA-sequencing and western blot analysis of the two other major human isoforms of UP-frameshift proteins, UPF1 and UPF2 showed no significant upregulation in *MYBPC3*$_{trunc}$ patients, however, a downregulation on protein level in AS-patients (Supplement Fig. 3). Thus, we assume that UPF3B upregulation is a specific mechanism in *MYBPC3*$_{trunc}$ patients.

3.5. Accumulation of UPF3B at the Z-disc in HCM-patient and donor cardiac tissue

Our results indicate that increased expression of UPF3B could play a specific role in *MYBPC3*-NMD. Since it has been reported previously, that sarcomeric proteins are translated directly at the sarcomeres [44], localization of NMD-components in sarcomeres could be relevant for efficient *MYBPC3*$_{trunc}$ mRNA degradation. Therefore, we visualized UPF1, UPF2, and UPF3B localization in cardiac tissue cryosections from three donors (H89, H108, and H113; Fig. 4A, B) and two patients (H45 and H84; Fig. 4C and D) by immunofluorescence in direct co-staining with α-actinin and DAPI. UPF1 showed strong accumulation in nuclei and a cytoplasmic stain with some indication of striations (Fig. 4A, upper panels). UPF2-fluorescence was essentially not detected in nuclei but showed a clearly distinguishable striated pattern (Fig. 4A middle panels). Interestingly, UPF3B immunofluorescence staining presented distinct dots, which also formed a clear striated pattern (Fig. 4A, lower panels). Only minor localization in nuclei was observed. Line profiles of UPF1, 2, and 3B fluorescence signals in comparison to α-actinin allowed to identify their position relative to the *Z*-disc (Fig. 4B). UPF1 and 2 showed striated patterns which opposed α-actinin, indicating localization in the A-band/H-zone. UPF3B showed a different pattern than the other two NMD-proteins. It showed overlapping peaks with α-actinin of around 1.8–2.0 μm distance between each peak which supports localization of UPF3B at the Z-discs (Fig. 4B, right panel). No substantial difference in UPF-localization between patient and donor cardiac tissue was found (compare Fig. 4A and B to C and D).

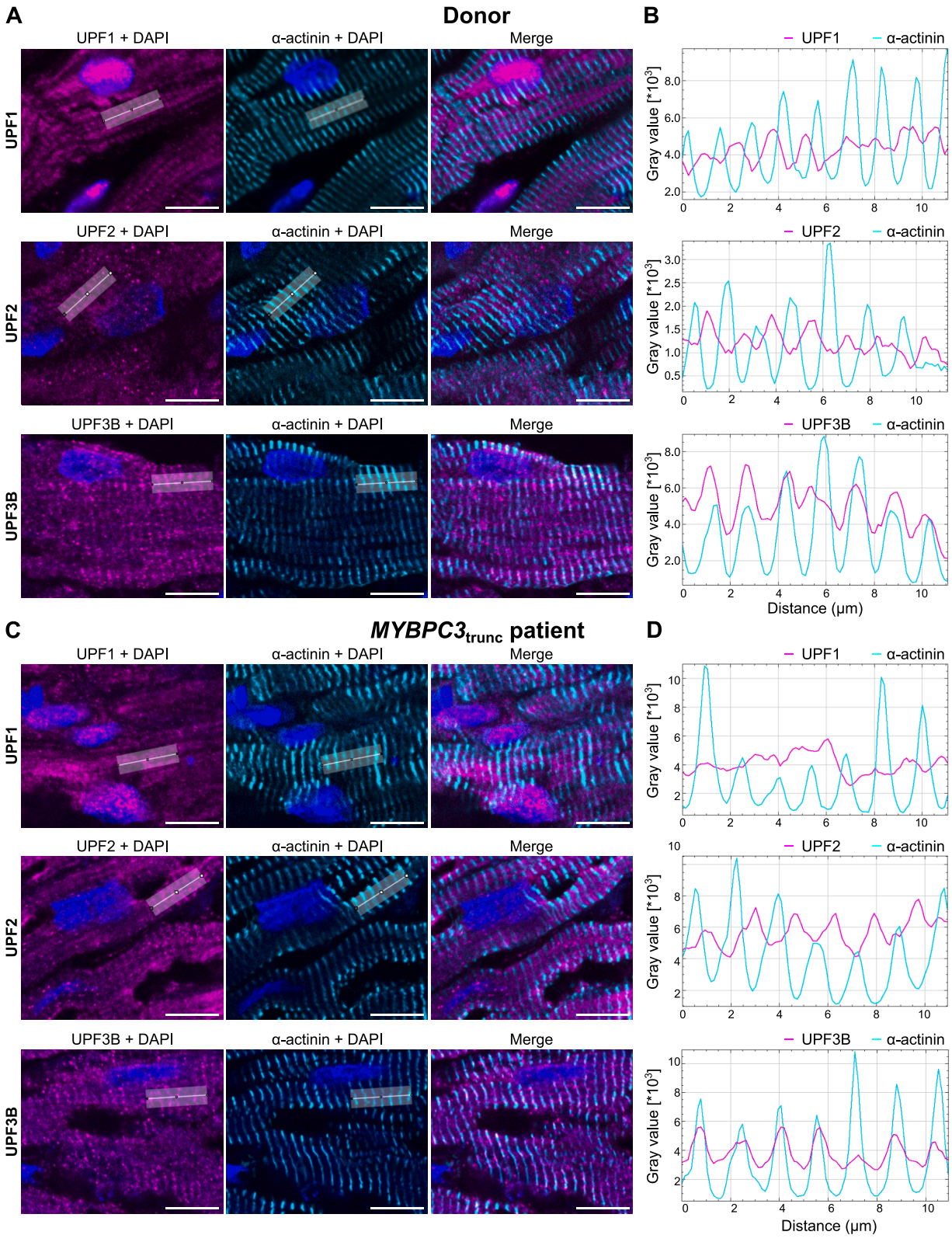

Fig. 4. UPF3B accumulates at the *Z*-disc in HCM-patient and donor cardiac tissue.
Left ventricular tissue cryosections (5 µm) from donor and *MYBPC3*$_{trunc}$ patient H84 were immunofluorescently co-stained with antibodies against UPF1, UPF2 or UPF3B each together with α-actinin. Images were taken by confocal laser scanning microscopy. **A** Donor cardiac tissue cryosections. Left images show a merge of either UPF1, UPF2 or UPF3B (magenta) with DAPI (blue), middle images a merge of α-actinin (cyan) and DAPI and right images a merge of all analyzed fluorescence. **B** Line profiles for UPF1, UPF2, UPF3B and α-actinin fluorescence from white boxes indicated in **A**. **C** Cardiac tissue cryosections from *MYBPC3*$_{trunc}$ patient H84. Images are arranged as described in **A**. **D** Line profiles for UPF1, UPF2, UPF3B and α-actinin fluorescence from white boxes indicated in **C**. Scale bars in all images represent 10 µm. (For interpretation of the references to colour in this figure legend, the reader is referred to the web version of this article.)

4. Discussion

Truncation mutations are the most common HCM-causing mutations in *MYBPC3* [3]. However, it is not completely understood how disease development is induced by heterozygous *MYBPC3* truncation mutations. In many cases, these truncation mutations lead to cMyBP-C haploinsufficiency [6–8,11]. In the literature there is consensus that cMyBP-C haploinsufficiency is established either by degradation of mutant mRNA via the nonsense mediated mRNA decay pathway [7,34,45,46] or by rapid degradation of truncated cMyBP-C fragments via the ubiquitin proteasome system [12,13]. However, experimental evidence for the involvement of NMD in degradation of mutated *MYBPC3*-mRNA is limited to a study in cMyBP-C knock-in mice [16] and a recent study in iPSC-CMs with *MYBPC3* PTC-mutations [47] but has not been shown in human myocardial samples. In this study, we analyzed *MYBPC3*-expression from transcription to protein level in *MYBPC3*$_{trunc}$ patients in comparison to heart-healthy donor samples and patients, which developed left ventricular hypertrophy without sarcomeric mutation but due to outflow obstruction caused by aortic stenosis (AS). We used samples of these patients to discriminate between alterations due to hypertrophy and alterations caused by *MYBPC3* truncation mutations. We found that cMyBP-C haploinsufficiency in *MYBPC3*$_{trunc}$ patients most likely results from the degradation of mutant *MYBPC3*-mRNA by NMD. We provide evidence for upregulation of NMD-associated factor UPF3B in *MYBPC3*$_{trunc}$ patients. Therefore, UPF3B could be involved in NMD of mutant *MYBPC3*-mRNA.

We chose a patient cohort of *MYBPC3*$_{trunc}$ patients with different truncation mutations for our study and found a significant reduction of cMyBP-C in all *MYBPC3*$_{trunc}$ patients compared to donors and to AS-patients. We show reduced cMyBP-C in *MYBPC3*$_{trunc}$ patients in relation to two different sarcomeric proteins, α-actinin as a protein of the *Z*-disc and cTnI as a protein of the thin filament, indicating disturbance of the strictly regulated sarcomeric stoichiometry (reviewed in [42]). In addition, we detected no truncated cMyBP-C fragments in the analyzed *MYBPC3*$_{trunc}$ patients in this and a previous study [40]. Thus, all patients in our study displayed haploinsufficiency, even though to a different extent ranging from 59% to 80% cMyBP-C content as compared to donors.

Reduction in cMyBP-C could be caused at different stages of protein biosynthesis. Thus, we examined transcriptional activity of the *MYBPC3*-gene, and *MYBPC3*-transcript levels in comparison to the protein level. We found an average increase of transcriptional activity for *MYBPC3* and *TNNI3* in *MYBPC3*$_{trunc}$ patients compared to donor samples. This could imply a compensatory effect at transcriptional level as reaction to reduced amounts of *MYBPC3*-mRNA and/or cMyBP-C protein. However, AS-patients also showed a comparable increase in transcriptional activity for both sarcomeric genes. This indicates that the overall increase in transcriptional activity is most likely due to a higher demand of sarcomeric proteins caused by hypertrophic growth of the hearts, and that it is no sole effect in *MYBPC3*$_{trunc}$ patients. In line with this assumption, the increased transcriptional activity did not restore *MYBPC3*-mRNA levels in HCM-patients. Conversely, qPCR quantification and RNA-sequencing analysis showed a significant decrease of *MYBPC3*-mRNA in HCM- but not in AS-patients. These results are in line with other groups reporting a decrease of *MYBPC3*-mRNA in *MYBPC3*$_{trunc}$ patients and iPSC-CMs with *MYBPC3* truncation mutations [8,48]. *MYBPC3*-reduction is presumably driven by decline of mutant mRNA, as shown by substantially decreased fractions of mutant mRNA in all patients. Most patients showed fractions below 10% and extremely low read numbers. Our finding that the relative level of *MYBPC3*-mRNA in each patient did not correlate with transcriptional activity but with cMyBP-C protein levels supports this conclusion. Thus, at least in the analyzed patients, haploinsufficiency is most likely already established at the mRNA level, presumably by degradation of mutant *MYBPC3*-mRNA due to efficient NMD. We additionally suppose, that it is not significantly regulated by the ubiquitin proteasome system (UPS). Involvement of UPS has been deduced from the finding that patients showed mutant transcripts but no detectable levels of truncated protein [6,7,9,10] and that inhibition of UPS leads to increased occurrence of mutated proteins [13]. In addition, dysfunction of the UPS was shown in different mouse models and cell culture models of cMyBP-C truncations, resulting in the assumption that the UPS is saturated by chronic degradation of truncated proteins [49,50]. However, we did neither detect substantial levels of mutant mRNA nor indications for differential regulation of the UPS-pathway in HCM-patients in the RNA-sequencing.

One exception was patient H84, where we detected 25% of mutant transcript. Interestingly, we also detected comparably high read counts of wildtype transcripts for this intron (37 reads) and also donors and other patients showed read counts ranging from 50 to 179 reads for this intron, which corresponds to 9–17% of total *MYBPC3*-mRNA which was not properly spliced at this intron. This suggests that the intron bears a rather weak splice site. However, the remaining intron will cause a PTC irrespective of the mutation, which seems to be ineffectively targeted by NMD. Therefore, the lack of truncated protein in both, donors and patients, could be regulated by the UPS, however, not dependent on the truncation mutation.

A possible reason for ineffective NMD at this position could be the rather long distance between PTC and the downstream EJC of 252 bp (Supplement Table 4). We examined whether the experienced variable degrees of *MYBPC3* and cMyBP-C reduction in the *MYBPC3*$_{trunc}$-patients might be due to different mechanisms of NMD-activation, which can be regulated by the closeness of the PTC to the poly(A) tail competing also with the EJC-dependent NMD [51,52]. However, we did not detect direct association of distance between PTC and downstream EJC with level of reduction in *MYBPC3*-mRNA, cMyBP-C protein or with fraction or read counts of mutant mRNA (Supplement Table 4). This suggests that mutated mRNAs of all analyzed *MYBPC3*$_{trunc}$-patients are degraded by the same NMD-pathway.

Seeger et al. previously reported an upregulation of the NMD-pathway in iPSC-CMs with cMyBP-C mutation p.R943x compared to isogenic control [37]. Furthermore, NMD-inhibition has been shown to increase the amount of *MYBPC3* nonsense transcripts and truncated cMyBP-C in iPSC-CMs and in mice with *MYBPC3* truncation mutations [16,47]. A constant demand on the NMD in patients with *MYBPC3* truncation mutation may result in upregulation of NMD-components. In addition, an increase in gene expression due to hypertrophic growth could increase NMD-demand regardless of PTC-containing *MYBPC3*-mRNAs. RNA-sequencing and GSEA revealed enrichment of the NMD-pathway in *MYBPC3*$_{trunc}$ patients compared to donors and NMD-specific genes are also upregulated in *MYBPC3*$_{trunc}$ patients in comparison to AS-patients. This suggests that upregulation of NMD-genes is not caused by hypertrophic growth per se but more likely due to degradation of PTC-containing *MYBPC3*-mRNAs via the NMD-pathway. However, dysregulated NMD-protein composition as well as a high demand on the NMD due to mutated *MYBPC3*-transcripts could still impact NMD-function and lead to accumulation of other PTC-containing transcripts from splice variants and finally truncated proteins [53]. Analyzing our RNA-sequencing data with the IsoformSwitchAnalyzeR tool did not reveal an increase of PTC-containing transcripts in the *MYBPC3*$_{trunc}$ patients compared to donors. This indicates that NMD is not exhausted in *MYBPC3*$_{trunc}$ patients and efficiently degrades PTC-containing transcripts including mutated *MYBPC3*-mRNA. Among the regulated NMD-specific genes, we identified the regulator of nonsense mediated decay Up-frameshift protein 3B (*UPF3B*, UPF3B) to be upregulated in *MYBPC3*$_{trunc}$ patients on mRNA and protein level when compared to donors and AS-patients. In contrast, UPF1 and UPF2 were not regulated in *MYBPC3*$_{trunc}$ patients.

Lewis and colleagues showed that several sarcomeric transcripts are transported to the *Z*-disc of the sarcomeres for translation [44]. Since mutant *MYBPC3*-mRNA seems to be targeted by NMD in *MYBPC3*$_{trunc}$ patients, degradation of the mutated transcripts could take place at the *Z*-discs as NMD depends on a first round of translation. This would

require localization of NMD-components at the sarcomeres, either associated to mRNA or to the Z-disc itself. Immunofluorescent staining of UPF3B revealed accumulation of UPF3B at the Z-discs. It has been shown that UPF3B shuttles between the nucleus and the cytoplasm [54,55] and that UPF3B-associated mRNA degradation is triggered in the cytoplasm [56]. In line with this, we detected some UPF3B within nuclei and in the cytoplasm not localized at the *Z*-discs, even though the majority seems to be located at the Z-discs. Based on the assumption that *MYBPC3*-mRNA is translated at the Z-disc, we hypothesize that PTC-containing mRNAs could be degraded via NMD in a UPF3B-dependent manner. Wildtype cMyBP-C in contrast would be translated at the Z-disc and subsequently transported to the A-band for incorporation into the sarcomere.

In contrast, UPF1 was localized in high levels in the nuclei, which presumably represents chromatin-bound UPF1 [19]. In addition, we detected UPF1-signals in the cytoplasm. In some areas, we detected a slight accumulation in the A-band. However, also areas without distinct striation pattern were found. As expected, UPF2 was found not found in nuclei. It accumulated in the A-band region and did not co-localize with the *Z*-discs.

The distinct localization of the UPF-proteins in CMs may be due to their different roles in PTC-transcript degradation. Localization of UPF3B at the Z-discs, the presumed place of sarcomere protein translation, could suggest a specific role in sarcomeric protein quality control. Interestingly, localization of UPFs was comparable in patients and donors suggesting that NMD uses the same pathways in donors and *MYBPC3*$_{trunc}$ patients. Since immunofluorescence analysis is not quantitative, we could not assess potential changes in UPF3B expression at the Z-discs. However, we can rule out that HCM leads to significantly altered localization of UPF-proteins. The increased UPF3B-protein expression determined by western blot could hint to higher levels of UPF3B at the Z-discs of HCM-patients.

5. Conclusions

The aim of our study was the identification of mechanisms that could underlie haploinsufficiency development in HCM-patients with *MYBPC3*$_{trunc}$ mutations. Our results indicate that NMD, not UPS, is the major pathway which leads to mutant *MYBPC3*-mRNA degradation and thus reduction in total cMyBP-C protein. Since most studies on NMD-involvement in HCM have been performed in mouse or cell culture models so far, our results from human cardiac tissue provide valuable insights into the pathology in humans. Furthermore, our study associates upregulation of NMD-associated factor UPF3B with haploinsufficiency in *MYBPC3*$_{trunc}$ patients and shows its localization at the Z-discs, the presumed site of sarcomeric protein translation. UPF3B could thus provide a novel target for investigations on cMyBP-C haploinsufficiency aiming at new therapeutic approaches that specifically influence NMD-functionality in HCM-patients.

Author contribution

VB and JM designed the research. VB, KK, and AD performed experiments. EP, AZ, MK, and OD-B contributed to data acquisition and analysis. DH-K, SL, CR, and AP provided patient or donor tissue. VB, JM, and TK wrote the manuscript. All authors contributed to the article and approved the submitted version.

Data availability

All available data are incorporated into this article and its online supplementary material. The RNA-sequencing data discussed in this publication have been deposited in NCBI's Gene Expression Omnibus [41] and are accessible through GEO Series accession number GSE230585 (https://www.ncbi.nlm.nih.gov/geo/query/acc.cgi?acc=GSE230585).

Acknowledgments

The Authors thank Sophie Nafe and Ilka Kröber (Institute for Molecular and Cell Physiology, Hannover Medical School) for excellent technical assistance and Britta Keyser (formerly Department for Human Genetics, Hannover Medical School) for sequence analysis of HCM-genes in patients and donors.

Funding

This work was supported by the Deutsche Forschungsgemeinschaft with grants KR1187/22-1, KR1187/22-2 and KR1187/21-2 to TK and MO2238/2-2 to JM and by ERA-CVD SCALE to JM.

Declaration of Competing Interest

None.

Declaration of Generative AI and AI-assisted technologies in the writing process

AI-assisted technology was not used in the preparation of the work.

Appendix A. Supplementary data

Supplementary data to this article can be found online at https://doi.org/10.1016/j.yjmcc.2023.09.008.

References

[1] R. Walsh, R. Buchan, A. Wilk, S. John, L.E. Felkin, K.L. Thomson, T.H. Chiaw, C. Chin, W. Loong, C.J. Pua, C. Raphael, S. Prasad, P.J. Barton, B. Funke, H. Watkins, J.S. Ware, S.A. Cook, Defining the genetic architecture of hypertrophic cardiomyopathy: re-evaluating the role of non-sarcomeric genes, Eur. Heart J. 38 (2017) 3461–3468, https://doi.org/10.1093/eurheartj/ehw603.

[2] P. Richard, P. Charron, L. Carrier, C. Ledeuil, T. Cheav, C. Pichereau, A. Benaiche, R. Isnard, O. Dubourg, M. Burban, J. Gueffet, A. Millaire, M. Desnos, K. Schwartz, B. Hainque, M. Komajda, Hypertrophic cardiomyopathy distribution of disease genes, Spectrum of mutations, and implications for a molecular diagnosis strategy, Circulation. 107 (2003) 2227–2232, https://doi.org/10.1161/01.CIR.0000066323.15244.54.

[3] A.A. Alfares, M.A. Kelly, G. McDermott, B.H. Funke, M.S. Lebo, S.B. Baxter, J. Shen, H.M. McLaughlin, E.H. Clark, L.J. Babb, S.W. Cox, S.R. Depalma, C.Y. Ho, J. G. Seidman, C.E. Seidman, H.L. Rehm, Results of clinical genetic testing of 2,912 probands with hypertrophic cardiomyopathy: expanded panels offer limited additional sensitivity, Genet. Med. 17 (2015) 880–888, https://doi.org/10.1038/gim.2014.205.

[4] L. Carrier, G. Bonne, E. Bährend, B. Yu, P. Richard, F. Niel, B. Hainque, C. Cruaud, F. Gary, S. Labeit, J.B. Bouhour, O. Dubourg, M. Desnos, A.A. Hagège, R.J. Trent, M. Komajda, M. Fiszman, K. Schwartz, Organization and sequence of human cardiac myosin binding protein C gene (MYBPC3) and identification of mutations predicted to produce truncated proteins in familial hypertrophic cardiomyopathy, Circ. Res. 80 (1997) 427–434, https://doi.org/10.1161/01.res.0000435859.24609.b3.

[5] P. Richard, E. Villard, P. Charron, R. Isnard, The genetic bases of cardiomyopathies, J. Am. Coll. Cardiol. 48 (2006) A79–A89, https://doi.org/10.1016/j.jacc.2006.09.014.

[6] S. Marston, O.N. Copeland, A. Jacques, K. Livesey, V. Tsang, W.J. Mckenna, S. Jalilzadeh, S. Carballo, C. Redwood, H. Watkins, Evidence from human Myectomy samples that MYBPC3 mutations cause hypertrophic cardiomyopathy through Haploinsufficiency, Circ. Res. 105 (2009) 219–222, https://doi.org/10.1161/CIRCRESAHA.109.202440.

[7] S.J. van Dijk, D. Dooijes, C. Remedios, M. Michels, J.M.J. Lamers, S. Winegrad, S. Schlossarek, L. Carrier, F.J. Cate, G.J.M. Stienen, J. van der Velden, Cardiac myosin-binding protein C mutations and hypertrophic cardiomyopathy, Circulation. 119 (2009) 1473–1484, https://doi.org/10.1161/CIRCULATIONAHA.108.838672.

[8] R.Y. Parbhudayal, A.R. Garra, M.J.W. Götte, M. Michels, J. Pei, M. Harakalova, F. W. Asselbergs, A.C. van Rossum, J. van der Velden, D.W.D. Kuster, Variable cardiac myosin binding protein-C expression in the myofilaments due to MYBPC3 mutations in hypertrophic cardiomyopathy, J. Mol. Cell. Cardiol. 123 (2018) 59–63, https://doi.org/10.1016/j.yjmcc.2018.08.023.

[9] J.A. Moolman, S. Reith, U.I. Kerstin, S. Bailey, M. Gautel, B. Jeschke, C. Fischer, J. Ochs, W.J. McKenna, H. Klues, H.P. Vosberg, A newly created splice donor site in exon 25 of the MyBP-C gene is responsible for inherited hypertrophic cardiomyopathy with incomplete disease penetrance, Circulation. 101 (2000) 1396–1402, https://doi.org/10.1161/01.CIR.101.12.1396.

[10] W. Rottbauer, M. Gautel, J. Zehelein, S. Labeit, W.M. Franz, C. Fischer, B. Vollrath, G. Mall, R. Dietz, W. Kübler, H.A. Katus, Novel splice donor site mutation in the cardiac myosin-binding protein- C gene in familial hypertrophic cardiomyopathy. Characterization of cardiac transcript and protein, J. Clin. Invest. 100 (1997) 475–482, https://doi.org/10.1172/JCI119555.

[11] S.J. van Dijk, E.R. Paalberends, A. Najafi, M. Michels, S. Sadayappan, L. Carrier, N. M. Boontje, D.W.D. Kuster, M. Van Slegtenhorst, D. Dooijes, C. Dos Remedios, F. J. Cate, G.J.M. Stienen, J. Van Der Velden, Contractile dysfunction irrespective of the mutant protein in human hypertrophic cardiomyopathy with normal systolic function, Circ. Heart Fail. 5 (2012) 36–46, https://doi.org/10.1161/CIRCHEARTFAILURE.111.963702.

[12] A. Sarikas, L. Carrier, C. Schenke, D. Doll, J. Flavigny, K.S. Lindenberg, T. Eschenhagen, O. Zolk, Impairment of the ubiquitin-proteasome system by truncated cardiac myosin binding protein C mutants, Cardiovasc. Res. 66 (2005) 33–44, https://doi.org/10.1016/j.cardiores.2005.01.004.

[13] U. Bahrudin, H. Morisaki, T. Morisaki, H. Ninomiya, K. Higaki, E. Nanba, O. Igawa, S. Takashima, E. Mizuta, J. Miake, Y. Yamamoto, Y. Shirayoshi, M. Kitakaze, L. Carrier, I. Hisatome, Ubiquitin-proteasome system impairment caused by a missense cardiac myosin-binding protein C mutation and associated with cardiac dysfunction in hypertrophic cardiomyopathy, J. Mol. Biol. 384 (2008) 896–907, https://doi.org/10.1016/j.jmb.2008.09.070.

[14] T. Kurosaki, L.E. Maquat, Nonsense-mediated mRNA decay in humans at a glance, J. Cell Sci. 129 (2016) 461–467, https://doi.org/10.1242/jcs.181008.

[15] L.E. Maquat, Nonsense-mediated mRNA decay in mammals, J. Cell Sci. 118 (2005) 1773–1776, https://doi.org/10.1242/jcs.01701.

[16] N. Vignier, S. Schlossarek, B. Fraysse, G. Mearini, E. Krämer, H. Pointu, N. Mougenot, J. Guiard, R. Reimer, H. Hohenberg, K. Schwartz, M. Vernet, T. Eschenhagen, L. Carrier, Nonsense-mediated mrna decay and ubiquitin-proteasome system regulate cardiac myosin-binding protein c mutant levels in cardiomyopathic mice, Circ. Res. 105 (2009) 239–248, https://doi.org/10.1161/CIRCRESAHA.109.201251.

[17] Z. Yi, M. Sanjeev, G. Singh, The branched nature of the nonsense-mediated mRNA decay pathway, Trends Genet. 37 (2021) 143–159, https://doi.org/10.1016/j.tig.2020.08.010.

[18] W.K. Chan, L. Huang, J.P. Gudikote, Y.F. Chang, J.S. Imam, J.A. MacLean, M. F. Wilkinson, An alternative branch of the nonsense-mediated decay pathway, EMBO J. 26 (2007) 1820–1830, https://doi.org/10.1038/sj.emboj.7601628.

[19] D. Hong, T. Park, S. Jeong, Nuclear UPF1 is associated with chromatin for transcription-coupled RNA surveillance, Mol. Cell 42 (2019) 523–529, https://doi.org/10.14348/MOLCELLS.2019.0116.

[20] D. Zünd, A.R. Gruber, M. Zavolan, O. Mühlemann, Translation-dependent displacement of UPF1 from coding sequences causes its enrichment in 3′ UTRs, Nat. Struct. Mol. Biol. 20 (2013) 936–943, https://doi.org/10.1038/nsmb.2635.

[21] T. Kurosaki, L.E. Maquat, Rules that govern UPF1 binding to mRNA 3′ UTRs, Proc. Natl. Acad. Sci. U. S. A. 110 (2013) 3357–3362, https://doi.org/10.1073/pnas.1219908110.

[22] J.R. Hogg, S.P. Goff, Upf1 senses 3′UTR length to potentiate mRNA decay, Cell. 143 (2010) 379–389, https://doi.org/10.1016/j.cell.2010.10.005.Upf1.

[23] T. Kurosaki, W. Li, M. Hoque, M.W.L. Popp, D.N. Ermolenko, B. Tian, L.E. Maquat, A post-translational regulatory switch on UPF1 controls targeted mRNA degradation, Genes Dev. 28 (2014) 1900–1916, https://doi.org/10.1101/gad.245506.114.

[24] H. Le Hir, E. Izaurralde, L.E. Maquat, M.J. Moore, The spliceosome deposits multiple proteins 20-24 nucleotides upstream of mRNA exon-exon junctions, EMBO J. 19 (2000) 6860–6869, https://doi.org/10.1093/emboj/19.24.6860.

[25] H. Le Hir, D. Gatfield, E. Izaurralde, M.J. Moore, The exon-exon junction complex provides a binding platform for factors involved in mRNA export and nonsense-mediated mRNA decay, EMBO J. 20 (2001) 4987–4997, https://doi.org/10.1093/emboj/20.17.4987.

[26] X. Sun, M.P. Moriarty, E.L. Maquat, Nonsense-mediated decay of glutathione peroxidase 1 mRNA in the cytoplasm depends on intron position, EMBO J. 19 (2000) 4734–4744, https://doi.org/10.1093/emboj/19.17.4734.

[27] B. Deka, P. Chandra, K.K. Singh, Functional roles of human up-frameshift suppressor 3 (UPF3) proteins: from nonsense-mediated mRNA decay to neurodevelopmental disorders, Biochimie. 180 (2021) 10–22, https://doi.org/10.1016/j.biochi.2020.10.011.

[28] N.H. Gehring, J.B. Kunz, G. Neu-Yilik, S. Breit, M.H. Viegas, M.W. Hentze, A. E. Kulozik, Exon-junction complex components specify distinct routes of nonsense-mediated mRNA decay with differential cofactor requirements, Mol. Cell 20 (2005) 65–75, https://doi.org/10.1016/j.molcel.2005.08.012.

[29] H. Chamieh, L. Ballut, F. Bonneau, H. Le Hir, NMD factors UPF2 and UPF3 bridge UPF1 to the exon junction complex and stimulate its RNA helicase activity, Nat. Struct. Mol. Biol. 15 (2008) 85–93, https://doi.org/10.1038/nsmb1330.

[30] S. Lykke-Andersen, T.H. Jensen, Nonsense-mediated mRNA decay: an intricate machinery that shapes transcriptomes, Nat. Rev. Mol. Cell Biol. 16 (2015) 665–677, https://doi.org/10.1038/nrm4063.

[31] F. Lejeune, Nonsense-mediated mRNA decay at the crossroads of many cellular pathways, BMB Rep. 50 (2017) 175–185, https://doi.org/10.5483/BMBRep.2017.50.4.015.

[32] L.F. Lareau, A.N. Brooks, D.A.W. Soergel, Q. Meng, S.E. Brenner, The coupling of alternative splicing and nonsense-mediated mRNA decay, Adv. Exp. Med. Biol. 15 (2007) 190–211, https://doi.org/10.1007/978-0-387-77374-2_12.

[33] L.B. Gardner, Hypoxic inhibition of nonsense-mediated RNA decay regulates gene expression and the integrated stress response, Mol. Cell. Biol. 28 (2008) 3729–3741, https://doi.org/10.1128/mcb.02284-07.

[34] A.S. Helms, F.M. Davis, D. Coleman, S.N. Bartolone, A.A. Glazier, F. Pagani, J. M. Yob, S. Sadayappan, E. Pedersen, R. Lyons, M.V. Westfall, R. Jones, M. W. Russell, S.M. Day, Sarcomere mutation-specific expression patterns in human hypertrophic cardiomyopathy, Circ. Cardiovasc. Genet. 7 (2014) 434–443, https://doi.org/10.1161/CIRCGENETICS.113.000448.

[35] J.L. Theis, J.M. Bos, J.D. Theis, D.V. Miller, J.A. Dearani, H.V. Schaff, B.J. Gersh, S. R. Ommen, R.L. Moss, M.J. Ackerman, Expression patterns of cardiac myofilament proteins, Circ. Heart Fail. 2 (2009) 325–333, https://doi.org/10.1161/CIRCHEARTFAILURE.108.789735.

[36] L. Carrier, Making sense of inhibiting nonsense in hypertrophic cardiomyopathy, Circulation. 139 (2019) 812–814, https://doi.org/10.1161/CIRCULATIONAHA.118.037936.

[37] T. Seeger, R. Shrestha, C.K. Lam, C. Chen, W.L. Mckeithan, E. Lau, A. Wnorowski, G. McMullen, M. Greenhaw, J. Lee, A. Oikonomopoulos, S. Lee, H. Yang, M. Mercola, M. Wheeler, E.A. Ashley, F. Yang, I. Karakikes, J.C. Wu, A premature termination codon mutation in MYBPC3 causes hypertrophic cardiomyopathy via chronic activation of nonsense-mediated decay, Circulation. 139 (2019) 799–811, https://doi.org/10.1161/CIRCULATIONAHA.118.034624.A.

[38] WMA, World Medical Association Declaration of Helsinki, JAMA. 277 (1997) 925–926. doi:https://doi.org/10.1001/jama.1997.03540350075038.

[39] C.G. dos Remedios, A. Li, S. Lal, Non-sarcomeric causes of heart failure: a Sydney heart Bank perspective, Biophys. Rev. 10 (2018) 949–954, https://doi.org/10.1007/s12551-018-0444-1.

[40] V. Burkart, K. Kowalski, D. Aldag-Niebling, J. Beck, D.A. Frick, T. Holler, A. Radocaj, B. Piep, A. Zeug, D. Hilfiker-Kleiner, C.G. dos Remedios, J. van der Velden, J. Montag, T. Kraft, Transcriptional bursts and heterogeneity among cardiomyocytes in hypertrophic cardiomyopathy, Front. Cardiovasc. Med 9 (2022), https://doi.org/10.3389/fcvm.2022.987889.

[41] R. Edgar, M. Domrachev, A.E. Lash, Gene expression omnibus: NCBI gene expression and hybridization array data repository, Nucleic Acids Res. 30 (2002) 207–210, https://doi.org/10.1093/nar/30.1.207.

[42] S.P. Harris, R.G. Lyons, K.L. Bezold, In the thick of it: HCM-causing mutations in myosin binding proteins of the thick filament, Circ. Res. 108 (2011) 751–764, https://doi.org/10.1161/CIRCRESAHA.110.231670.

[43] K. Vitting-Seerup, A. Sandelin, B. Berger, IsoformSwitchAnalyzeR: analysis of changes in genome-wide patterns of alternative splicing and its functional consequences, Bioinformatics. 35 (2019) 4469–4471, https://doi.org/10.1093/bioinformatics/btz247.

[44] Y.E. Lewis, A. Moskovitz, M. Mutlak, J. Heineke, L.H. Caspi, I. Kehat, Localization of transcripts, translation, and degradation for spatiotemporal sarcomere maintenance, J. Mol. Cell. Cardiol. 116 (2018) 16–28, https://doi.org/10.1016/j.yjmcc.2018.01.012.

[45] L. Carrier, S. Schlossarek, M.S. Willis, T. Eschenhagen, The ubiquitin-proteasome system and nonsense-mediated mRNA decay in hypertrophic cardiomyopathy, Cardiovasc. Res. 85 (2010) 330–338, https://doi.org/10.1093/cvr/cvp247.

[46] L. Carrier, G. Mearini, K. Stathopoulou, F. Cuello, Cardiac myosin-binding protein C (MYBPC3) in cardiac pathophysiology, Gene. 573 (2015) 188–197, https://doi.org/10.1016/j.gene.2015.09.008.

[47] N.A. Warnecke, Disease Modelling and Molecular Therapy of Severe Cardiomyopathy in hiPSC-Derived Cardiomyocytes Carrying Bi-Allelic Truncating MYBPC3 Mutations, Universitätsklinikum Hamburg-Eppendorf, 2021. https://ediss.sub.uni-hamburg.de/handle/ediss/9407.

[48] A.S. Helms, V.T. Tang, T.S. O'Leary, S. Friedline, M. Wauchope, A. Arora, A. H. Wasserman, E.D. Smith, L.M. Lee, X.W. Wen, J.A. Shavit, A.P. Liu, M.J. Previs, S. M. Day, Effects of MYBPC3 loss-of-function mutations preceding hypertrophic cardiomyopathy, JCI Insight 5 (2020), https://doi.org/10.1172/jci.insight.133782.

[49] J.M. Predmore, P. Wang, F. Davis, S. Bartolone, M.V. Westfall, D.B. Dyke, F. Pagani, S.R. Powell, S.M. Day, Ubiquitin proteasome dysfunction in human hypertrophic and dilated cardiomyopathies, Circulation. 121 (2010) 997–1004, https://doi.org/10.1161/CIRCULATIONAHA.109.904557.

[50] T. Thottakara, F.W. Friedrich, S. Reischmann, S. Braumann, S. Schlossarek, E. Krämer, D. Juhr, H. Schlüter, J. van der Velden, J. Münch, M. Patten, T. Eschenhagen, C. Moog-Lutz, L. Carrier, The E3 ubiquitin ligase Asb2β is downregulated in a mouse model of hypertrophic cardiomyopathy and targets desmin for proteasomal degradation, J. Mol. Cell. Cardiol. 87 (2015) 214–224, https://doi.org/10.1016/j.yjmcc.2015.08.020.

[51] M. Bühler, S. Steiner, F. Mohn, A. Paillusson, O. Mühlemann, EJC-independent degradation of nonsense immunoglobulin-μ mRNA depends on 3′ UTR length, Nat. Struct. Mol. Biol. 13 (2006) 462–464, https://doi.org/10.1038/nsmb1081.

[52] G. Singh, I. Rebbapragada, J. Lykke-Andersen, A competition between stimulators and antagonists of Upf complex recruitment governs human nonsense-mediated mRNA decay, PLoS Biol. 6 (2008) 860–871, https://doi.org/10.1371/journal.pbio.0060111.

[53] D. Wallmeroth, J. Lackmann, S. Kueckelmann, J. Altmüller, C. Dieterich, V. Boehm, N.H. Gehring, Human UPF3A and UPF3B enable fault-tolerant activation of nonsense-mediated mRNA decay, EMBO J. 41 (2022), https://doi.org/10.15252/embj.2021109191.

[54] G. Serin, A. Gersappe, J.D. Black, R. Aronoff, L.E. Maquat, Identification and characterization of human orthologues to Saccharomyces cerevisiae Upf2 protein and Upf3 protein (Caenorhabditis elegans SMG-4), Mol. Cell. Biol. 21 (2001) 209–223, https://doi.org/10.1128/MCB.21.1.209-223.2001.

[55] J. Lykke-Andersen, M. Di Shu, J.A. Steitz, Human Upf proteins target an mRNA for nonsense-mediated decay when downstream of a termination codon, Cell. 103 (2000) 1121–1131, https://doi.org/10.1016/S0092-8674(00)00214-2.
[56] G. Singh, S. Jakob, M.G. Kleedehn, J. Lykke-Andersen, Communication with the exon-junction complex and activation of nonsense-mediated decay by human Upf proteins occur in the cytoplasm, Mol. Cell 27 (2007) 780–792, https://doi.org/10.1016/j.molcel.2007.06.030.
[57] M. Schuldt, J. Pei, M. Harakalova, L.M. Dorsch, S. Schlossarek, M. Mokry, J. C. Knol, T.V. Pham, T. Schelfhorst, S.R. Piersma, C. dos Remedios, M. Dalinghaus, M. Michels, F.W. Asselbergs, M.-J. Moutin, L. Carrier, C.R. Jimenez, J. van der Velden, D.W.D. Kuster, Proteomic and functional studies reveal detyrosinated tubulin as treatment target in sarcomere mutation-induced hypertrophic cardiomyopathy, Circ. Hear. Fail. 14 (2021), https://doi.org/10.1161/CIRCHEARTFAILURE.120.007022.